# Enhanced efficiency and selectivity of carbon monoxide absorption by cuprous-based bimetallic deep eutectic solvents via iron activation

Wen-Qiang Gong [1], Zhang-Min Li [1], Xue-Rui Zhou, Jian-Fei Li, Yan Zhou, Ming-Shuai Sun, Wei Hui [*], Duan-Jian Tao [*]

*National Engineering Research Center for Carbohydrate Synthesis, Key Laboratory of Fluorine and Silicon for Energy Materials and Chemistry of Ministry of Education, School of Chemical Engineering, Jiangxi Normal University, Nanchang 330022 China*

ABSTRACT

The absorption/utilization of carbon monoxide (CO) is critical due to its wide application in chemical production processes (e.g., acylation), and its toxicity/environmental impact. However, traditional copper-ammonia solutions in industry have limitations such as the deactivation of copper ions and high viscosity, which hinder efficient CO absorption under atmospheric conditions. In this work, a series of low-viscosity bimetallic deep eutectic solvents (DESs) with high CO absorption capacity were developed by mixing metal chlorides with [Emim]Cl and CuCl in specific molar ratios. Comprehensive studies of their physical properties (density and viscosity) and CO absorption performance revealed that [Emim]Cl-CuCl-1.0FeCl$_3$ exhibited the lowest viscosity (57.4 cP) and a nearly equimolar CO absorption capacity (0.9 mol/mol). Moreover, the selectivity for CO/N$_2$ (730), CO/CO$_2$ (22), and CO/H$_2$ (52) at 298.2 K and 100 kPa was also satisfied. The data of Raman and FT-IR spectra demonstrated that FeCl$_3$ effectively activated cuprous sites in CuCl and significantly enhanced the CO absorption performance of cuprous-based bimetallic DESs. Furthermore, [Emim]Cl-CuCl-1.0FeCl$_3$ showed excellent reusability after six absorption–desorption cycles. Therefore, we believe that this work provides a route for the effective activation of cuprous sites in cuprous-based bimetallic DESs to achieve efficient and reversible CO absorption at atmospheric conditions.

## 1. Introduction

As well known, carbon monoxide (CO) is an asphyxiating gas that can bind to hemoglobin in the blood and may cause coma and/or toxic death in humans. [1–3] Meanwhile, the exhaust gases from incomplete combustion and the steelmaking industry contain a significant amount of CO, which may enhance the greenhouse effect and pose a serious safety risk to the environment. On the other hand, CO is a crucial feedstock gas for the carbonylation, acylation, hydroformylation, and Fischer-Tropsch synthesis reactions of various high-value fine chemicals. [4–7] The separation and reutilization of CO from industrial exhaust gases align with the principles of green and sustainable development. [8] However, the traditional cuprous-ammonia solution absorption method for CO absorption faces challenges such as the deactivation of cuprous (Cu(I)) sites due to disproportionation and subsequent pipeline blockage, which hinders the industrial development of the absorption and reutilization of CO. [9] Therefore, the design of

novel absorbents for CO absorption is crucial for the further development of this field.

Ionic liquids (ILs) [10–12] and deep eutectic solvents (DESs) [13–15] are among the most advanced solvents in the separation field. ILs are typically a bulky organic cation paired with an organic or inorganic anion, exhibiting low melting points and vapor pressure. [16,17] In contrast, DESs are mixtures of hydrogen bond donors and acceptors, which form complex hydrogen-bonded networks that provide enhanced solubility and sustainability. [18] It is noteworthy that most of the functions of ILs can also be found in DESs, which not only retain many of their advantages but also eliminate some of their limitations, such as toxicity, biocompatibility issues, and high cost. [19–21] At present, researchers have been developed a wide range of ILs and DESs systems for CO absorption. For example, Laurenczy et al. [22] quantified the CO absorption capacities of 37 different ILs and established a prediction method for the CO absorption capacities of similar ILs. Urtiaga and co-authors [23] designed an imidazolium chlorocuprate(I) IL ([Hmim]

---

[CuCl]) that facilitates CO absorption through coordination interactions between Cu(I) and CO. Furthermore, Tao et al. [24] reported a class of carbanion-functionalized IL ([$P_{4448}$][Pen]) for efficient CO absorption, with [$P_{4448}$][Pen] having achieved an absorption capacity of 0.046 mol/mol at 298.2 K and 100 kPa through the interaction between the activated carbanion sites and CO.

In recent years, ternary DESs systems for CO absorption have attracted great attention. For instance, Cui et al. reported Cu(I)-based ternary DESs ([HDEEA][Cl] + CuCl + EG) for CO absorption by activating Cu(I) in DESs via hydroxyl groups and ethylene glycol. [25] Tao et al. further reported a Cu(I)-based DESs absorbent ([EimH][OAc]-0.6CuOAc) for rapid and selective CO absorption at 293.2 K and 1.0 bar, and later developed a new class of Cu(I)-based ternary DESs ([BimH][Cl]-CuCl-1.0ZnCl$_2$) capable of CO absorption at high temperature (353.2 K). [26,27] Specifically, the ZnCl$_2$ moiety in [BimH]Cl-CuCl-1.0ZnCl$_2$ forms a weak interaction with the Cl$^-$ of the CuCl moiety, thereby weakening the Cu − Cl bonds and achieving Cu(I) activation. Overall, the activation level of Cu(I) sites in Cu(I)-based ILs and DESs is relatively low, which leads to insufficient utilization of Cu(I) sites in these absorbents. Moreover, high viscosity is another issue that limits the efficient CO absorption of most Cu(I)-based absorbents. Thus, improving CO absorption in low-viscosity Cu(I)-based DESs necessitates identifying more effective methods to activate Cu(I), with known strategies including the use of various metal ions to achieve Cu(I) activation.

Herein, a novel metal-activated cuprous-based bimetallic DESs with low viscosity was developed through the mixing of metal chloride with [Emim]Cl and CuCl at specific molar ratios. The density and viscosity properties and CO absorption performance of cuprous-based bimetallic DESs were systematically evaluated. The results show that [Emim]Cl-CuCl-1.0FeCl$_3$ has lower viscosity and higher CO absorption capacity compared to previously reported cuprous-based absorbents, suggesting that it improves the CO absorption efficiency and reusability of Cu(I)-based DESs. Specifically, the CO absorption capacity of [Emim]Cl-CuCl-1.0FeCl$_3$ was as high as 0.90 mol CO per mole of Cu(I), and the ideal adsorbed solution theory (IAST) selectivity of CO/CO$_2$, CO/H$_2$, and CO/N$_2$ was also satisfied. Furthermore, the CO absorption mechanism of [Emim]Cl-CuCl-1.0FeCl$_3$ was investigated, and the activation effect of different metal chloride salts on Cu(I) was examined using FT-IR and Raman. The results demonstrate that iron salt plays a crucial role in Cu(I) activation in these cuprous-based bimetallic DESs.
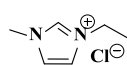
## 2. Experimental

### 2.1. Materials

Carbon monoxide (CO, 99.999 %), carbon dioxide (CO$_2$, 99.999 %), hydrogen (H$_2$, 99.999 %), and nitrogen (N$_2$, 99.999 %) were purchased from Jiangxi Huahong Special Gas Co., Ltd., Jiangxi Province, China. Ferric chloride (FeCl$_3$, 99.9 %), zinc chloride (ZnCl$_2$, 98.0 %), cuprous chloride (CuCl, 99.0 %), aluminum chloride (AlCl$_3$, 99.0 %), 3-methyl-1-octylimidazolium chloride ([Omim]Cl, 99.0 %) and 1-ethyl-3-methylimidazolium chloride ([Emim]Cl, 99.0 %) were purchased from Shanghai Macklin Biochemical Technology Co., Ltd., Shanghai Municipality, China. Except for CuCl, all other experimental reagents can be used directly without the necessity for further purification treatments.

### 2.2. Preparation of Cu(I)-based bimetallic DESs

In this work, Cu(I)-based bimetallic DESs were prepared by the heating and mixing method [28]. The typical preparation detail for the [Emim]Cl-CuCl-$x$FeCl$_3$ ($x$ = 0.5, 1.0, 1.5) are as follows: [Emim]Cl and FeCl$_3$ were mixed in molar ratios of 1:$x$ at room temperature and stirred for 2 h until homogeneous single-phase solutions ([Emim]Cl-$x$FeCl$_3$) were obtained. Subsequently, [Emim]Cl-$x$FeCl$_3$ mixture was combined with CuCl in a molar ratio of 1:1 under vacuum and at 333.2 K, resulting in the formation of the Fe-activated Cu(I)-based bimetallic DES, denoted

**Table 1**
Cu(I)-based bimetallic DESs with the different metal salts.

| Metal-activated Cu(I)-based bimetallic DESs | Component 1 | Metal salts | Cuprous salt |
|---|---|---|---|
| | $\overset{\ominus}{\underset{Cl}{\overset{\oplus}{N \diagdown N}}}$ | | |
| [Emim]Cl-CuCl-1.0FeCl$_3$ | [Emim]Cl | FeCl$_3$ | CuCl |
| [Emim]Cl-CuCl-1.0AlCl$_3$ | [Emim]Cl | AlCl$_3$ | CuCl |
| [Emim]Cl-CuCl-1.0ZnCl$_2$ | [Emim]Cl | ZnCl$_2$ | CuCl |
| [Emim]Cl-CuCl | [Emim]Cl | − | CuCl |

as [Emim]Cl-CuCl-$x$FeCl$_3$. Several other Cu(I)-based bimetallic DESs were prepared using a similar method. Table 1 shows the compositions of three metal-activated Cu(I)-based bimetallic DESs.

### 2.3. Characterization of Cu(I)-based bimetallic DESs

The density of Cu(I)-based bimetallic DESs were measured using an Anton Paar DMA 4500 automatic densitometer. The viscosity values of Cu(I)-based bimetallic DESs were obtained using a Brookfield DV II + Pro viscometer. Thermogravimetric analysis curves were generated by a PerkinElmer Diamond TG/DTA analyzer under nitrogen atmosphere protection. The apparatus Fourier-Transform infrared spectrometer (FT-IR, Nicolet 6700) and Raman spectrometer (LabRAM HR) were employed to obtain the FT-IR and Raman spectra, respectively.

### 2.4. Evaluation CO absorption capacity

The CO absorption data of Cu(I)-based bimetallic DESs were determined by a homemade dual chamber experimental setup, which is the same as the device reported in our previous works (Figure S1). [29–31] The gas absorption unit comprises two gas chambers made of 316 L stainless steel with different volumes, two pressure sensors, a circulating water bath, and a magnetic stirrer. A larger volume gas chamber (gas storage chamber, V$_1$) is used to store the gas under test. A smaller volume chamber (absorption chamber, V$_2$) is used for CO absorption experiments. The experimental temperature is kept constant by the operation of a circulating water bath apparatus. A certain mass of Cu(I)-based bimetallic DESs was weighed and placed in the absorption chamber, and the chamber was maintained under vacuum. CO was transferred from the gas cylinder to the storage chamber (P$_1$). When the pressure values in the two chambers remain constant for at least 1h, it can be considered that the absorbent has reached equilibrium for CO absorption. At this time, the pressures in the storage chamber and absorption chamber were denoted P$_1'$ and P$_2$, respectively. The CO absorption capacity of Cu(I)-based bimetallic DESs was calculated by measuring the pressure change between the dual chambers before and after CO absorption. The relevant calculation formula of CO absorption capacity (n) was shown in equation (1):

$$n = \rho_1 V_1 - \rho_1' V_1 - \rho_2(V_2 - m/\rho_{DES}) \tag{1}$$

Where $\rho_1$ is the density of CO at T and P$_1$. $\rho_1'$ is the density of CO at T and P$_1'$. $\rho_2$ is the density of CO at T and P$_2$. $\rho_{DES}$ is the density of DES at T. To ensure the accuracy of the experimental results, the absorption capacity of CO was calculated by averaging three measurements. The selectivity of CO/N$_2$, CO/CO$_2$, and CO/H$_2$ was calculated using the IAST model constructed by Myers et al. [32,33] As shown in equation (2), n$_1$ and n$_2$ are the gas absorption capacities in the phase under the absorption equilibrium condition. P$_1$ and P$_2$ are the gas phase partial pressures in equilibrium.
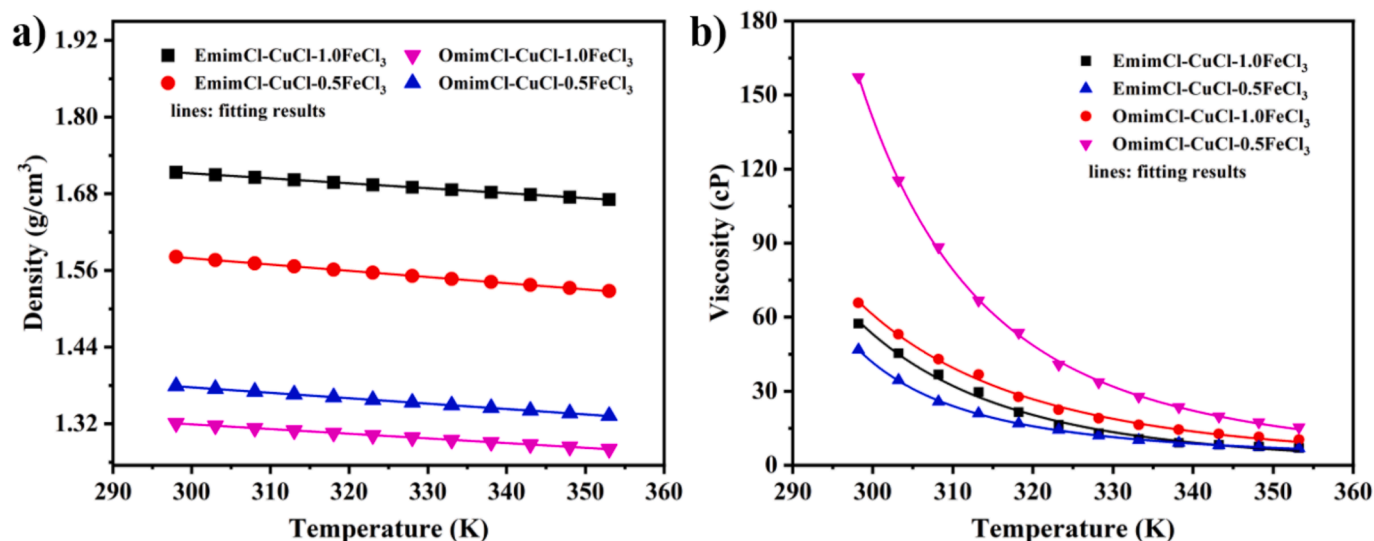
$$S = \frac{n_1/n_2}{p_1/p_2} \tag{2}$$

**Fig. 1.** Densities (a) and viscosities (b) curves of Cu(I)-based bimetallic DESs at different temperatures.
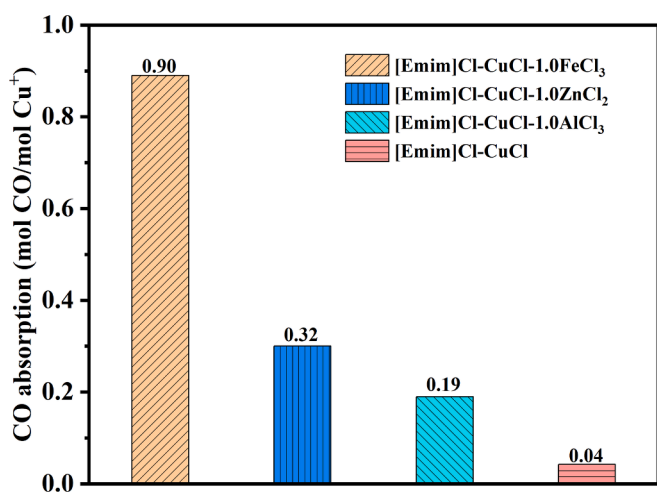


**Fig. 2.** The CO absorption capacity of Cu(I)-based bimetallic DESs with different metal chloride salts.

## 3. Results and Discussion

### 3.1. Physical properties and thermal stability

The densities and viscosities of liquid adsorbents are important physical parameters that have an important influence on their absorption capacity during CO absorption. Fig. 1 shows the trends in densities and viscosities of Cu(I)-based bimetallic DESs over a temperature range of 298.2 K to 353.2 K. Obviously, the density values of these Cu(I)-based bimetallic DESs decrease linearly with increasing temperature from 298.2 K to 353.2 K (Fig. 1a). Meanwhile, the viscosity values exhibit a nonlinear exponential decay with rising temperature (Fig. 1b). Notably, the viscosity of [Emim]Cl-CuCl-1.0FeCl$_3$ was measured to be 57.4 cP at 298.2 K, which implies that it has low mass transfer resistance during CO absorption. Furthermore, the viscosity and density data of these Cu(I)-based bimetallic DESs were fitted and calculated using equations (3) and (4), respectively ($R^2 > 0.99$). The relevant fitting parameters are listed in Table S1. Besides, the thermal stability of Cu(I)-based bimetallic DESs was evaluated, and the results are shown Figure S2. The results show that the decomposition temperature of [Emim]Cl-CuCl-1.0FeCl$_3$ reached up to 609 K, which means that the Cu(I)-based bimetallic DESs absorbent still maintains excellent stability for CO

**Table 2**
Viscosities of different metal-activated Cu(I)-based bimetallic DESs at 298.2 K.

| Absorbents | Temperature (K) | Viscosity (cP) |
|---|---|---|
| [Emim]Cl-CuCl-1.0FeCl$_3$ | 298.2 | 57 |
| [Emim]Cl-CuCl-1.0AlCl$_3$ | 298.2 | $> 1 \times 10^4$ |
| [Emim]Cl-CuCl-1.0ZnCl$_2$ | 298.2 | $> 1 \times 10^4$ |

absorption–desorption at high temperatures.

$$\rho = A + BT \qquad (3)$$

$$\eta = \eta_0 \exp\left(\frac{D}{T - T_0}\right) \qquad (4)$$

### 3.2. CO absorption performance

To evaluate the effect of various metal chloride salts on the CO absorption performance in Cu(I)-based bimetallic DESs, their CO absorption capacities were investigated at 298.2 K and 100 kPa. As shown in Fig. 2, the CO absorption capacity of [Emim]Cl-CuCl-1.0FeCl$_3$ was the highest (0.90 mol/mol, based on Cu(I) sites). In comparison, the absorption capacities of [Emim]Cl-CuCl-1.0ZnCl$_2$, [Emim]Cl-CuCl-1.0AlCl$_3$, and [Emim]Cl-CuCl were 0.32, 0.19, and 0.04 mol/mol, respectively. These results support that Fe metal salts are beneficial in activating Cu(I) sites and increase the CO absorption capacity of the Cu(I)-based DESs. Meanwhile, the viscosity values of the Cu(I)-based bimetallic DESs were measured and are listed in Table 2. It is found

**Table 3**
The CO absorption capacities of Fe-activated Cu(I)-based bimetallic DESs at 298.2 K and 100 kPa.

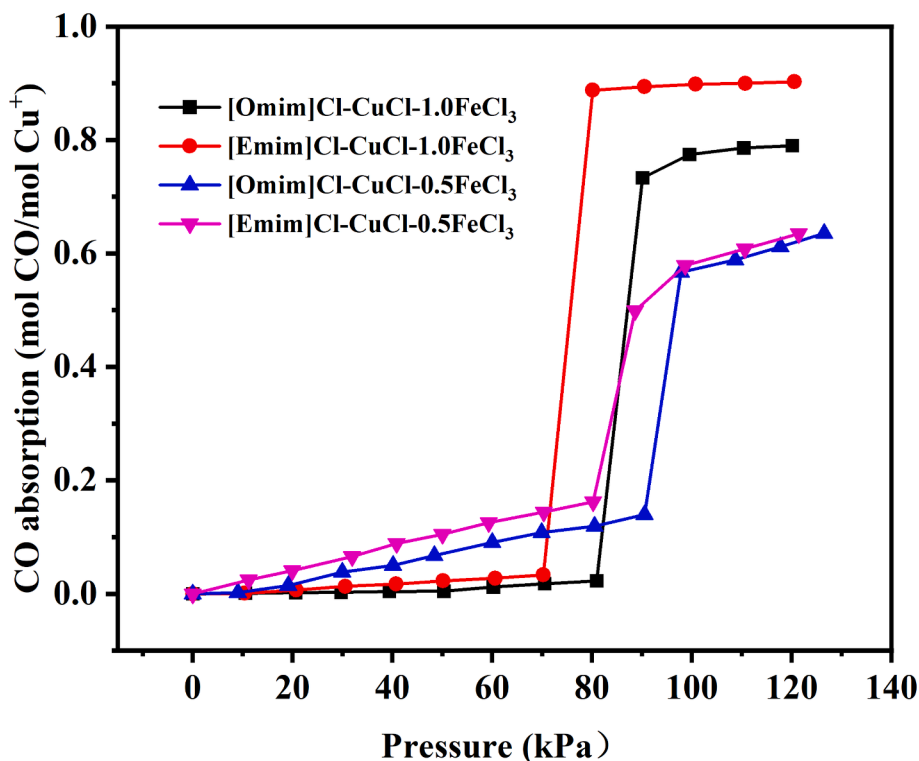| Absorbents | Temperature (K) | Pressure (kPa) | CO absorption capacities | |
|---|---|---|---|---|
| | | | mmol/g | mol/mol |
| [Emim]Cl-CuCl-1.0FeCl$_3$ | 298.2 | 100 | 2.20 | 0.90 |
| [Omim]Cl-CuCl-1.0FeCl$_3$ | 298.2 | 100 | 1.50 | 0.77 |
| [Emim]Cl-CuCl-0.5FeCl$_3$ | 298.2 | 100 | 1.77 | 0.58 |
| [Omim]Cl-CuCl-0.5FeCl$_3$ | 298.2 | 100 | 1.47 | 0.57 |

**Fig. 3.** The CO absorption isotherms of Cu(I)-based bimetallic DESs with different molar ratios at 298.2 K.

that the viscosity values of [Emim]Cl-CuCl-1.0AlCl$_3$ ($> 10^4$ cP) and [Emim]Cl-CuCl-1.0ZnCl$_2$ ($> 10^4$ cP) were significantly higher than that of [Emim]Cl-CuCl-1.0FeCl$_3$ (57.4 cP). The result cooperated with the CO absorption data, suggest that the lower viscosity of [Emim]Cl-CuCl-1.0FeCl$_3$ is conducive to mass transfer and CO absorption. For comparison, the higher viscosities of [Emim]Cl-CuCl-1.0AlCl$_3$ and [Emim]Cl-CuCl-1.0ZnCl$_2$ increase the mass transfer resistance, leading to reduced CO absorption capacity.

Subsequently, the effect of Fe-Cu ratios and the alkyl chains of imidazolium salts in Cu(I)-based DESs on CO absorption capacities were evaluated, the Fe-Cu ratios of Cu(I)-based DESs were tuned, and their absorption performances were measured under the same condition. As shown in Table 3, the CO absorption capacity of [Emim]Cl-CuCl-$x$FeCl$_3$ and [Omim]Cl-CuCl-$x$FeCl$_3$ ($x$ = 0.5, 1.0, and 1.5) absorbents is on the order of [Emim]Cl-CuCl-1.0FeCl$_3$ > [Omim]Cl-CuCl-1.0FeCl$_3$ > [Emim]Cl-CuCl-0.5FeCl$_3$ > [Omim]Cl-CuCl-0.5FeCl$_3$. In addition, the synthesized [Emim]Cl-CuCl-1.5FeCl$_3$ and [Omim]Cl-CuCl-1.5FeCl were in a solid phase at room temperature, which prevents it impossible to measure CO absorption data. It was found that increasing Fe-Cu ratios in Cu(I)-based DESs have a positive impact on CO absorption, which was attributed to the coordination between FeCl$_3$ and Cl$^-$ of cuprous, thereby promoting the activation of Cu(I) sites. However, the results also showed that the use of [Omim]Cl as a component in these Cu(I)-based DESs was less effective for CO absorption. The longer side chain of [Omim]Cl component leads to a higher viscosity of [Omim]Cl-CuCl-0.5FeCl$_3$ (157.3 cP) compared to [Emim]Cl-CuCl-0.5FeCl$_3$ (46.8 cP), which limited mass transfer for CO absorption in the liquid phase. Overall, the above results supported that the effective activation of CuCl and the reduced viscosity of Cu(I)-based DESs are crucial for improving the CO absorption capacity.

In addition, the CO absorption isotherms of the four DESs were measured at 298.2 K to further explore their CO absorption behaviors, and the results are shown in Fig. 3. Interestingly, the CO absorption capacities of Cu(I)-based DESs show a clear upward trend with the increase in CO partial pressure. The CO absorption processes are divided into three stages: the initial stage shows a linear increase, followed by a

**Table 4**
Comparison of CO absorption capacity at 100 kPa by different absorbents.

| Entry | Absorbents | Temperature (K) | Absorption capacity (mol/mol) | Ref. |
|---|---|---|---|---|
| 1 | [Emim]Cl-CuCl-1.0FeCl$_3$ | 298.2 | 0.90 | This work |
| 2 | [P$_{4448}$][Pen] | 298.2 | 0.05 | [24] |
| 3 | [bmim][CH$_3$SO$_4$] | 303.2 | $2.6 \times 10^{-3}$ | [43] |
| 4 | [Bmim][Tf$_2$N] | 303.2 | $1.5 \times 10^{-3}$ | [22] |
| 5 | [Bmim][BF$_4$] | 295.2 | $2.9 \times 10^{-3}$ | [22] |
| 6 | [Bmim][PF$_6$] | 295.2 | $3.0 \times 10^{-3}$ | [22] |
| 7 | [EimH][CuCl$_2$] | 293.2 | 0.12 | [35] |
| 8 | [EimH]OAc-0.6[CuOAc] | 293.2 | 0.42 | [26] |
| 9 | [TEA][CuCl$_2$] | 303.2 | 0.08 | [44] |
| 10 | [BimH]Cl-ZnCl$_2$-CuCl | 353.2 | 0.08 | [27] |
| 11 | [Hmim][CuCl$_2$] | 303.2 | 0.02 | [23] |
| 12 | [HDEEA][Cl] + CuCl + EG(1:1:4) | 293.2 | 0.20 | [25] |

sudden increase in CO absorption capacity in the medium pressure range, and finally CO absorption capacity gradually reaches saturation in the near-atmospheric pressure range. Specifically, the linear increase in the CO absorption isotherm for the [Emim]Cl-CuCl-1.0FeCl$_3$ within the pressure range from 0 to 70 kPa indicates that physical absorption predominantly occurs in this range. However, as the pressure further increases to 80 kPa, the CO absorption capacity exhibits a significant rise from 0.03 mol/mol to 0.88 mol/mol, which means that chemical absorption plays a dominant role at relatively high CO partial pressures. In other words, the transition from single physical to physicochemical absorption occurs as more CO molecules form coordination interactions with Cu(I) sites. Meanwhile, similar dual absorption behavior of CO by absorbents has been reported in the literature. [34] Therefore, the superior CO absorption capacity of [Emim]Cl-CuCl-1.0FeCl$_3$ can be primarily attributed to the coordinated interaction of Cu(I) sites with CO molecules.
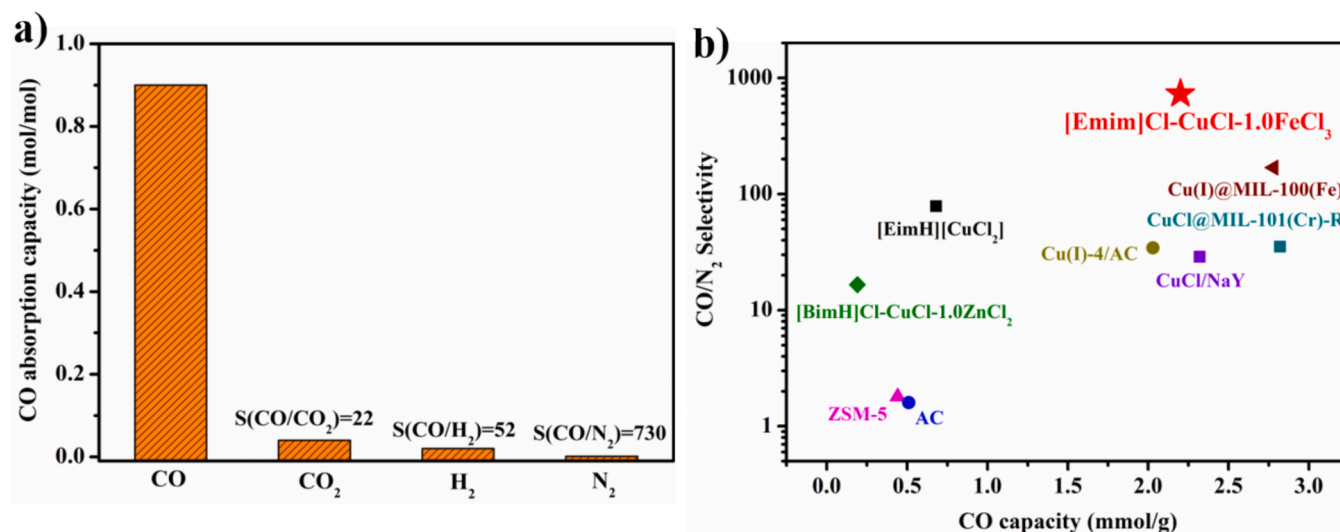
**Fig. 4.** (a) The absorption capacities of CO, $CO_2$, $H_2$, and $N_2$ in [Emim]Cl-CuCl-1.0FeCl$_3$ at 298.2 K and 1.0 bar and (b) Comparison with CO/$N_2$ selectivities of other adsorbents reported in the literature.

### 3.3. Comparison with other absorbents

The CO absorption capacity of the [Emim]Cl-CuCl-1.0FeCl$_3$ absorbent in this work was compared with those of several other ILs and DESs reported in the literature, and the results are summarized in Table 4. It is obvious that [Emim]Cl-CuCl-1.0FeCl$_3$ (0.90 mol/mol) exhibits an outstanding CO absorption capacity under similar conditions. For example, the absorption capacity of [Emim]Cl-CuCl-1.0FeCl$_3$ is higher than ILs without Cu(I), and its performance is 18 to 600 times that of ILs such as $[P_{4448}][Pen]$, $[Bmim][CH_3SO_4]$, $[Bmim][Tf_2N]$, $[Bmim][BF_4]$, and $[Bmim][PF_6]$ (Table 3, entries 2–6). Furthermore, the optimal adsorbent of [Emim]Cl-CuCl-1.0FeCl$_3$ also showed significantly higher CO absorption capacity than most Cu(I)-based IL and Cu(I)-based bimetallic DESs (Table 3, entries 7–12). Such as, the absorption capacity of [Emim]Cl-CuCl-1.0FeCl$_3$ was 7.5 to 45 times that of [EimH][CuCl$_2$], [TEA][CuCl$_2$], [Hmim][CuCl$_2$], [BimH]Cl-ZnCl$_2$-CuCl, and [HDEEA][Cl] + CuCl + EG(1:1:4). These results suggest that FeCl$_3$ successfully improves the activation efficiency of Cu(I) sites in Cu(I)-based DESs, making its CO absorption performance significantly better than previously reported Cu(I)-based absorbents. At the same time, this

also means that [Emim]Cl-CuCl-1.0FeCl$_3$ adsorbent has great application potential in CO capture and separation processes and can play an important role in industrial CO treatment and environmental protection in the future.

### 3.4. IAST selectivity

The selective separation of guest gases using adsorbents is one of important criterion for evaluating their application potential. The CO-containing exhaust gas from the industry typically composes other gas components, such as $N_2$, $CO_2$, and $H_2$. The absorption capacities of $N_2$, $CO_2$, and $H_2$ on [Emim]Cl-CuCl-1.0FeCl$_3$ were determined at 298.2 K and 100 kPa, as illustrated in Fig. 4a. It was found that the absorption capacities of $N_2$, $CO_2$, and $H_2$ by [Emim]Cl-CuCl-1.0FeCl$_3$ were found to be $1.23 \times 10^{-3}$, $4 \times 10^{-2}$, and $2 \times 10^{-2}$ mol/mol, respectively. The IAST selectivity of CO/$N_2$, CO/$CO_2$, and CO/$H_2$ was calculated using equation (2). The results found that the IAST selectivity for CO/$N_2$, CO/$CO_2$, and CO/$H_2$ could reach 730, 22, and 52, respectively. Compared to other adsorbents for CO absorption, [Emim]Cl-CuCl-1.0FeCl$_3$ exhibited significantly higher CO/$N_2$ selectivity (Fig. 4b). [27,35–41] This
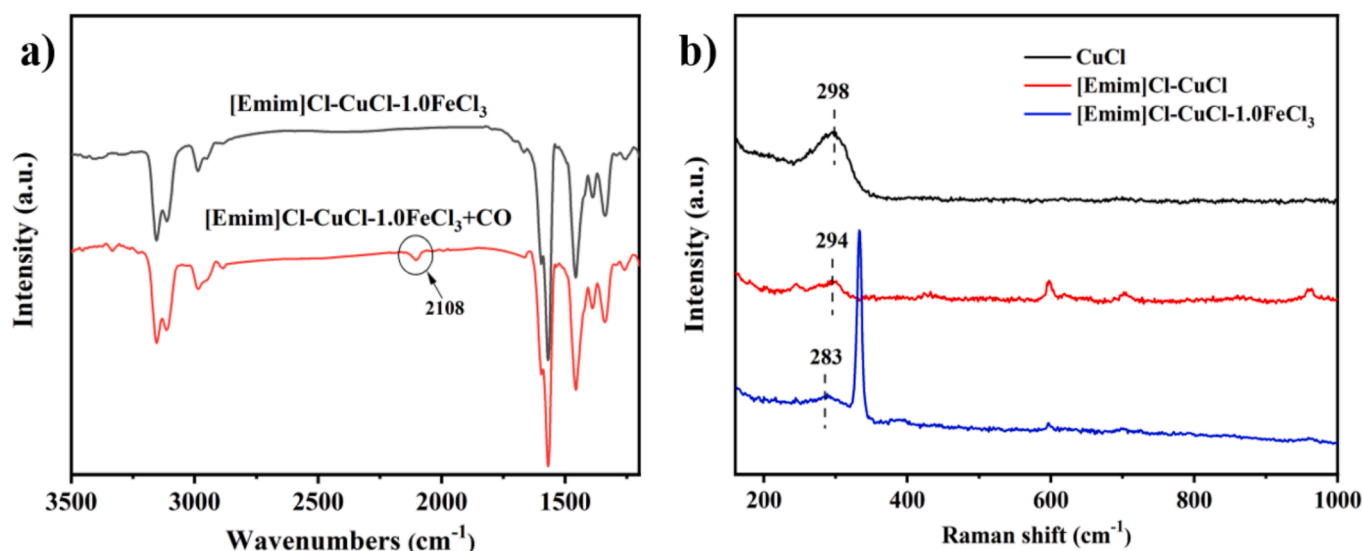


**Fig. 5.** (a) FT-IR spectra of [Emim]Cl-CuCl-1.0FeCl$_3$ before and after absorption of CO. (b) Raman spectra of [Emim]Cl-CuCl-1.0FeCl$_3$, [Emim]Cl-CuCl, and CuCl.
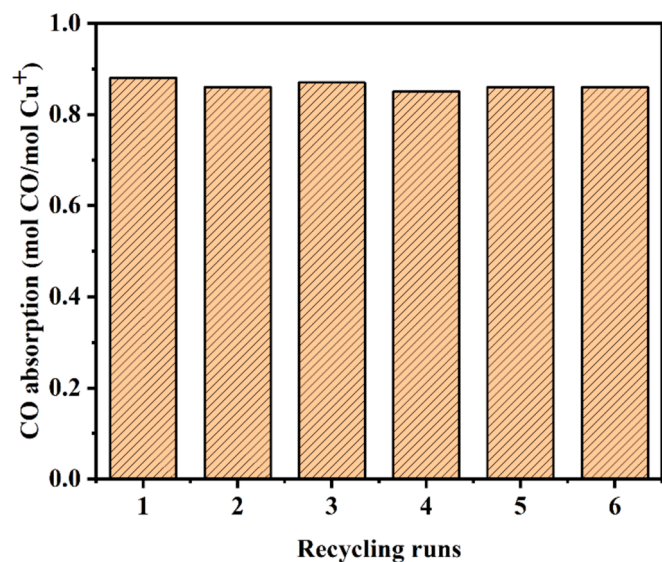
**Fig. 6.** Reusability of [Emim]Cl-CuCl-1.0FeCl$_3$ for CO absorption.

suggests that [Emim]Cl-CuCl-1.0FeCl$_3$ has the potential for the selective recovery of CO from industrial exhaust gases.

### 3.5. Absorption mechanism

The characteristic peaks of [Emim]Cl-CuCl-1.0FeCl$_3$ before and after CO absorption were compared using FT-IR and Raman to validate the reliability of the adsorption behavior inferred from the experimental data. As shown in Fig. 5a, the absorption peak at 2108 cm$^{-1}$ in [Emim] Cl-CuCl-1.0FeCl$_3$ after CO absorption ([Emim]Cl-CuCl-1.0FeCl$_3$ + CO), which was ascribed to the CO stretching vibration in the π-complex formed between it and CO. [26,34] Specifically, Cu(I) interact effectively with CO to form stable Cu(CO)$^+$ complexes, and this π-complexation has been verified by several previous studies. [26,27,34] In fact,

the red-shift of the CO stretching frequency from 2143 cm$^{-1}$ (free) to 2108 cm$^{-1}$ (π-complex), which further confirmed the presence of strong chemical absorption interaction between [Emim]Cl-CuCl-1.0FeCl$_3$ and CO molecules. Moreover, Raman also provided evidence that FeCl$_3$ enhanced the chemical interaction of Cu(I)-based bimetallic DES with CO molecules. It is well known that the characteristic peak of unactivated CuCl is located at 298 cm$^{-1}$. [42] However, the Cu-Cl in [Emim] Cl-CuCl and [Emim]Cl-CuCl-1.0FeCl$_3$ synthesized in this work both showed a peak red-shift trend, and the wavenumbers decreased to 294 cm$^{-1}$ and 283 cm$^{-1}$, respectively. These wavenumber shifts support that the [Emim]Cl component and FeCl$_3$ moiety can activate Cu(I) via coordination with Cl$^-$ in CuCl, which is consistent with previous literature results. [27,34,35] It should be noted that the Cu-Cl peak of [Emim]Cl-CuCl-1.0FeCl$_3$ was more shifted than that of [Emim]Cl-CuCl, which means that FeCl$_3$ moiety plays a more efficient role in the activation of Cu(I), while [Emim]Cl component plays a minor role. Furthermore, the CO adsorption isotherms (Fig. 3) show that the CO absorption capacity of [Emim]Cl-CuCl-$x$FeCl$_3$ increases significantly as the Fe-Cu ratio rises from 0.5 to 1.0. These results further support the positive impact of FeCl$_3$ and [Emim]Cl moieties on improving the activation efficiency of Cu(I) sites. As a result, the CO absorption capacity of the optimal [Emim] Cl-CuCl-1.0FeCl$_3$ adsorbent exhibited a CO absorption capacity of 0.90 mol/mol under atmospheric conditions. This remarkable performance can be ascribed to the synergistic impact between [Emim]Cl and FeCl$_3$, which improves the activation efficiency of Cu(I) in Cu(I)-based bimetallic DESs.

### 3.6. Cycle performance

The long-term reversible of CO absorption ability of [Emim]Cl-CuCl-1.0FeCl$_3$ at 298.2 K and 100 kPa was tested to evaluate its industrial application potential in CO absorption and separation, and the results are shown in Fig. 6. It can be found that CO absorption capacities of [Emim]Cl-CuCl-1.0FeCl$_3$ still maintain the optimal performance after six CO absorption–desorption, which supports that this absorbent is effective in carrying out CO absorption and separation is reversible. Besides, the stability tests of CO uptake performance of [Emim] Cl-CuCl-
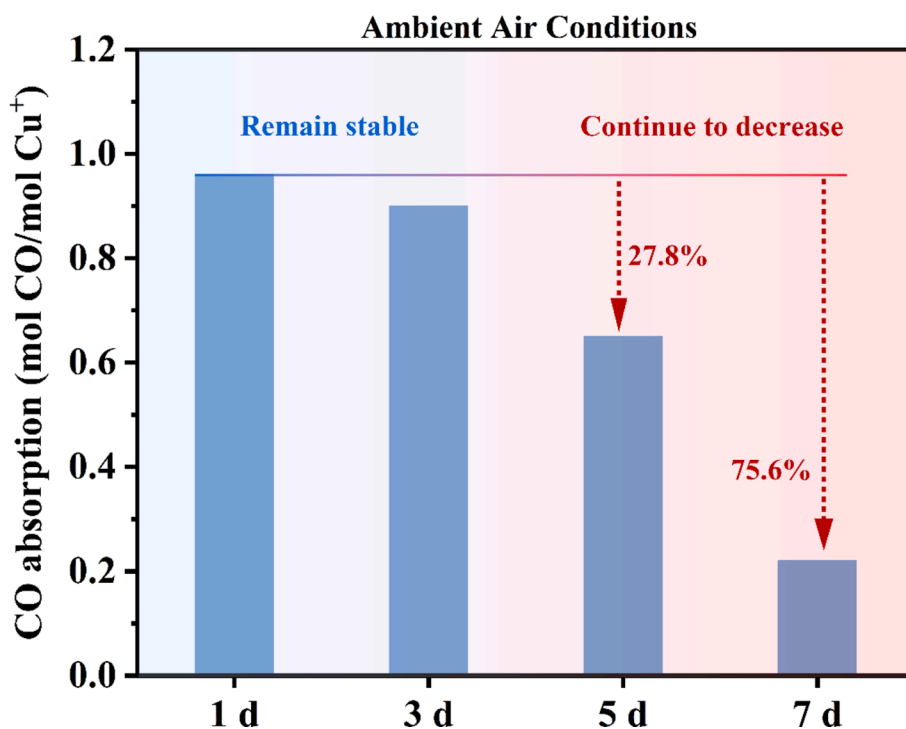


**Fig. 7.** Stability of CO absorption performance of [Emim]Cl-CuCl-1.0FeCl$_3$ under ambient air conditions at 298.2 K and 100 kPa.
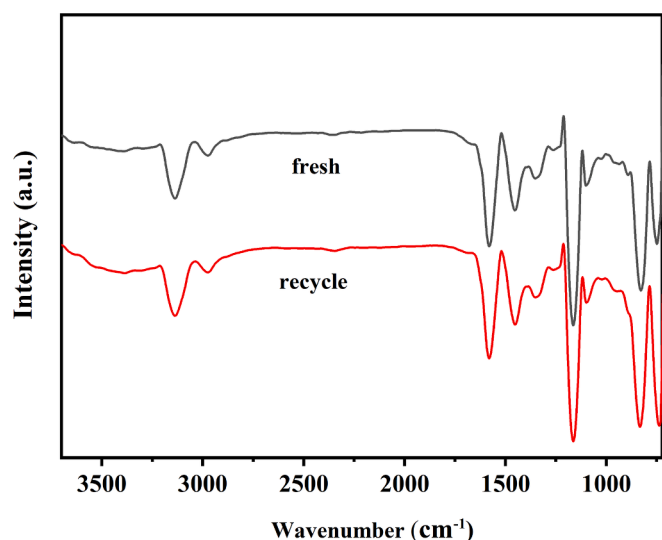
**Fig. 8.** FT-IR spectra of [Emim]Cl-CuCl-1.0FeCl$_3$ before and after cycle.

1.0FeCl$_3$ under ambient air conditions (see Fig. 7). The results show that the performance of [Emim] Cl-CuCl-1.0FeCl$_3$ underwent both a stable phase (1 and 3 days) and a subsequent continuous decline phase (5 and 7 days), which can be ascribed to the deactivation of Cu(I) sites caused by their interaction of oxygen and moisture in the air. Therefore, the stability test further corroborates the crucial role of Cu(I) sites in facilitating effective CO absorption. Moreover, the characteristic absorption bands of fresh and recycled [Emim]Cl-CuCl-1.0FeCl$_3$ were compared using the FT-IR, as shown in Fig. 8. Obviously, the FT-IR spectrum of the recovered absorbent [Emim]Cl-CuCl-1.0FeCl$_3$ is comparable to that of the fresh absorbent, implying that the absorbent remains structurally intact after six cycles. As a result, the results demonstrate that Cu(I)-based bimetallic DESs are highly efficient and reversible CO absorbents with excellent reusability and stability in CO absorption and separation.

## 4. Conclusion

In summary, we have successfully developed Cu(I)-based bimetallic DESs [Emim]Cl-CuCl-1.0FeCl$_3$ with low viscosity for efficient CO absorption at atmospheric conditions. The effects of Fe-Cu ratios and the alkyl chains of imidazolium salts on CO absorption capacities was evaluated, with increasing Fe-Cu ratios having a positive effect on CO absorption. However, the use of [Omim]Cl as a component in Cu(I)-based bimetallic DESs was less effective for CO absorption, as its longer side chain led to higher viscosity, which limited mass transfer for CO absorption in the liquid phase. Furthermore, the superior performance of the [Emim]Cl-CuCl-1.0FeCl$_3$ absorbent can be attributed to the role of FeCl$_3$ for activating Cu(I) sites in CuCl based on the results of spectra characterizations and experiments, in which an excellent CO absorption capacity (0.90 mol/mol) and selectivity (730, CO/N$_2$) at 298.2 K and 100 kPa was obtained. Its performance was 18 to 600 times higher than ILs without Cu(I) and significantly higher than most Cu(I)-based ILs and bimetallic DESs, suggesting its potential for selective CO recovery from industrial exhaust gases. In addition, the [Emim]Cl-CuCl-1.0FeCl$_3$ absorbent maintained excellent absorption performance after six absorption–desorption tests, indicating its potential long-term operational capability in industrial applications. Therefore, this work provides potential routes and directions for the future development of new and efficient CO absorption materials.

## CRediT authorship contribution statement

**Wen-Qiang Gong:** Investigation, Formal analysis. **Zhang-Min Li:** Methodology, Resources, Writing – original draft. **Xue-Rui Zhou:** Investigation, Validation. **Jian-Fei Li:** Visualization. **Yan Zhou:** Visualization. **Ming-Shuai Sun:** Validation. **Wei Hui:** Investigation, Writing – review & editing, Writing – original draft. **Duan-Jian Tao:** Conceptualization, Funding acquisition, Project administration, Supervision.

## Declaration of competing interest

The authors declare that they have no known competing financial interests or personal relationships that could have appeared to influence the work reported in this paper.

## Acknowledgments

## Appendix A. Supplementary data

Supplementary data to this article can be found online at https://doi.org/10.1016/j.seppur.2024.130079.

## Data availability

Data will be made available on request.

## References

[1] D. Gentile, R. Adams, M. Klatka, S. Bradberry, L. Gray, R. Thanacoody, G. Jackson, E.A. Sandilands, Carbon monoxide exposures reported to the uk national poisons information service: a 4-year study, J. Public Health 44 (3) (2022) 565–574.

[2] C. Mattiuzzi, G. Lippi, Worldwide epidemiology of carbon monoxide poisoning, Hum. Exp. Toxicol. 39 (4) (2020) 387–392.

[3] R.J. Chen, Y.H. Lee, T.H. Chen, Y.Y. Chen, Y.L. Yeh, C.P. Chang, C.C. Huang, H.R. Guo, Y.J. Wang, Carbon monoxide-triggered health effects: the important role of the inflammasome and its possible crosstalk with autophagy and exosomes, Arch. Toxicol. 95 (4) (2021) 1141–1159.

[4] H.K. Wu, F. Zhang, J.Y. Li, Z.R. Tang, Y.J. Xu, Photo-driven Fischer-Tropsch synthesis, J. Mater. Chem. A 8 (46) (2020) 24253–24266.

[5] D.X. Guan, G. Godard, S.M. Polas, R.P. Tooze, A.C. Whitwood, S.B. Duckett, Using para hydrogen induced polarization to study steps in the hydroformylation reaction, Dalton t. 48 (8) (2019) 2664–2675.

[6] C.L. Wang, N. Liu, X.Q. Wu, J.P. Qu, Y.F. Chen, Nickel-catalyzed regiodivergent acylzincation of styrenes with organozincs and CO, Chin. J. Chem. 42 (6) (2023) 599–604.

[7] L. Ying, Y. Han, B.E. Zhu, Y. Gao, Exploration of structure sensitivity of gold nanoparticles in low-temperature CO oxidation, Ind. Chem. Mater. 2 (2) (2024) 321–327.

[8] Z.Y. Yang, R.Z. Chen, L. Zhang, Y.H. Li, C.Z. Li, Recent progress in nickel single-atom catalysts for the electroreduction of CO$_2$ to CO, Ind. Chem, Mater, 2024.

[9] J.A. Hogendoorn, W.P.M.V. Swaaij, G.F. Versteeg, The absorption of carbon monoxide in COSORB solutions: absorption rate and capacity, Chem. Eng. J. 59 (3) (1995) 243–252.

[10] A. Hafizi, M. Rajabzadeh, M.H. Mokari, R. Khalifeh, Synthesis, property analysis and absorption efficiency of newly prepared tricationic ionic liquids for CO$_2$ absorption, J. Mol. Liq. 324 (2021) 115108.

[11] T. Makino, M. Kanakubo, NH$_3$ absorption in Brønsted acidic imidazolium- and ammonium-based ionic liquids, New J. Chem. 44 (47) (2020) 20665–20675.

[12] W.H. Tu, S.J. Zeng, Y. Bai, X.C. Zhang, H.F. Dong, X.P. Zhang, Theoretical insights into NH$_3$ absorption mechanisms with imidazolium-based protic ionic liquids, Ind. Chem. Mater. 1 (2023) 262–270.

[13] E.L. Smith, A.P. Abbott, K.S. Ryder, Deep eutectic solvents (DESs) and their applications, Chem. Rev. 114 (21) (2014) 11060–11082.

[14] G. García, S. Aparicio, R. Ullah, M. Atilhan, Deep eutectic solvents: physicochemical properties and gas separation applications, Energ. Fuel. 29 (4) (2015) 2616–2644.

[15] Y. Chen, T.C. Mu, Revisiting greenness of ionic liquids and deep eutectic solvents, Green Chem. Eng. 2 (2) (2021) 174–186.

[16] S.Y. Wen, L.Z. Zheng, X.M. Zhang, Y.T. Wu, Unveiling protic amino acid ionic liquids for the efficient capture of carbon dioxide, Chem. Commun. 60 (50) (2024) 6443–6446.

[17] H.L. Ning, M.Z. Shi, Q. Yang, J.W. Huang, X.M. Zhang, Y.T. Wu, K.C. Jie, Rational design of porous ionic liquids for coupling natural gas purification with waste gas conversion, Angew. Chem. Int. Ed. Engl. 62 (46) (2023) e202310741.

[18] D. Snigur, E.A. Azooz, O. Zhukovetska, O. Guzenko, W. Mortada, Low-density solvent-based liquid-liquid microextraction for separation of trace concentrations of different analytes, TrAC Trend. Anal. Chem. 167 (2023) 117260.

[19] R. Ahmadi, E.A. Azooz, Y. Yamini, A.M. Ramezani, Liquid-liquid microextraction techniques based on in-situ formation/decomposition of deep eutectic solvents, TrAC Trend. Anal. Chem. 161 (2023) 117019.

[20] R. Craveiro, I. Aroso, V. Flammia, T. Carvalho, M.T. Viciosa, M. Dionísio, S. Barreiros, R.L. Reis, A.R.C. Duarte, A. Paiva, Properties and thermal behavior of natural deep eutectic solvents, J Mol. Liq. 215 (2016) 534–540.

[21] F.A. Wannas, E.A. Azooz, A.A.S. Al-Mushhdi, I.A. Naguib, Ionic liquid-based cloud point extraction for spectrophotometric determination of copper in water and food samples using a novel imidazole derivative, J Food Compos. Anal. 135 (2024) 106638.

[22] C.A. Ohlin, P.J. Dyson, G. Laurenczy, Carbon monoxide solubility in ionic liquids: determination, prediction and relevance to hydroformylation, Chem. Commun. 9 (2004) 1070–1071.

[23] G. Zarca, I. Ortiz, A. Urtiaga, Kinetics of the carbon monoxide reactive absorption by an imidazolium chlorocuprate(I) ionic liquid, Chem. Eng. J. 252 (2014) 298–304.

[24] D.J. Tao, F.F. Chen, Z.Q. Tian, K. Huang, S.M. Mahurin, D.E. Jiang, S. Dai, Highly efficient carbon monoxide absorption by carbanion-functionalized ionic liquids through C-site interactions, Angew. Chem. Int. Ed. Engl. 56 (24) (2017) 6843–6847.

[25] G.K. Cui, K. Jiang, H. Liu, Y. Zhou, Z. Zhang, R. Zhang, H. Lu, Highly efficient CO removal by active cuprous-based ternary deep eutectic solvents [HDEEA][Cl] + CuCl + EG, Sep. Purif. Technol. 274 (2021) 118985.

[26] D.J. Tao, X.C. An, Z.T. Gao, Z.M. Li, Y. Zhou, Cuprous-based composite ionic liquids for the selective absorption of CO: experimental study and thermodynamic analysis, AIChE J. 68 (5) (2022) e17631.

[27] D.J. Tao, F. Qu, Z.M. Li, Y. Zhou, Promoted absorption of CO at high temperature by cuprous-based ternary deep eutectic solvents, AIChE J. 67 (2) (2020) e17106.

[28] N.M. Abdulhussein, N.M. Muslim, M.A. Hussien, E.A. Azooz, E.A.J. Al-Mulla, Green preconcentration procedures for the determination of aluminium in bottled beverages prior to electrothermal atomic absorption spectroscopy: A comparative study with environmental assessment tools, J Iran. Chem. Soc. 21 (5) (2024) 1203–1212.

[29] C. Tan, Z.M. Li, M.S. Sun, H. Guan, Y. Zhou, D.J. Tao, Sulfonated phenol–formaldehyde resins for highly efficient, selective, and reversible adsorption of NH₃, Ind. Eng. Chem. Res. 62 (3) (2023) 1542–1549.

[30] Z.M. Li, S.X. Zhu, F.F. Mao, Y. Zhou, W. Zhu, D.J. Tao, CTAB-controlled synthesis of phenolic resin-based nanofiber aerogels for highly efficient and reversible SO₂ absorption, Chem. Eng. J. 431 (2022) 133715.

[31] W.Q. Gong, X.L. Wu, Z.M. Li, Y. Zhou, W. Zhu, D.J. Tao, Sulfate ionic liquids impregnated 2D boron nitride nanosheets for trace SO₂ absorption with high capacity and selectivity, Sep. Purif. Technol. 270 (2021) 118824.

[32] A.L. Myers, Equation of state for adsorption of gases and their mixtures in porous materials, Adsorption 9 (2003) 9–16.

[33] A.L. Myers, J.M. Prausnitz, Thermodynamics of mixed-gas adsorption, AIChE J. 11 (1) (1965) 121–127.

[34] S.X. Zhu, Z.M. Li, W.Q. Gong, Z.T. Gao, H. Guan, M.S. Sun, Y. Zhou, D.J. Tao, Equimolar CO absorption by cuprous-based quaternary deep eutectic solvents, Ind. Eng. Chem. Res. 62 (6) (2023) 2937–2943.

[35] Y.M. Liu, Z.Q. Tian, F. Qu, Y. Zhou, Y. Liu, D.J. Tao, Tuning ion-pair interaction in cuprous-based protic ionic liquids for significantly improved CO absorption, ACS Sustain. Chem. Eng. 7 (13) (2019) 11894–11900.

[36] F.V.S. Lopes, C.A. Grande, A.M. Ribeiro, J.M. Loureiro, O. Evaggelos, V. Nikolakis, A.E. Rodrigues, Adsorption of H₂, CO₂, CH₄, CO, N₂ and H₂O in activated carbon and zeolite for hydrogen production, Sep. Sci. Technol. 44 (5) (2009) 1045–1073.

[37] G. Sethia, G.P. Dangi, A.L. Jetwani, R.S. Somani, H.C. Bajaj, R.V. Jasra, Equilibrium and dynamic adsorption of carbon monoxide and nitrogen on ZSM-5 with different SiO₂/Al₂O₃ ratio, Sep. Sci. Technol. 45 (3) (2010) 413–420.

[38] C. Xue, W. Hao, W. Cheng, J. Ma, R. Li, CO adsorption performance of CuCl/ activated carbon by simultaneous reduction-dispersion of mixed Cu(II) salts, Materials 12 (10) (2019) 1605.

[39] Y.C. Xie, J.P. Zhang, J.G. Qiu, X.Z. Tong, J.P. Fu, G. Yang, H.J. Yan, Y.Q. Tang, Zeolites modified by CuCl for separating CO from gas mixtures containing CO₂, Adsorption 3 (1996) 27–32.

[40] J.J. Peng, S.K. Xian, J. Xiao, Y. Huang, Q.B. Xia, H.H. Wang, Z. Li, A supported Cu (I)@MIL-100(Fe) adsorbent with high CO adsorption capacity and CO/N₂ selectivity, Chem. Eng. J. 270 (2015) 282–289.

[41] T.K. Vo, J.H. Kim, H.T. Kwon, J. Kim, Cost-effective and eco-friendly synthesis of MIL-101(Cr) from waste hexavalent chromium and its application for carbon monoxide separation, J. Ind. Eng. Chem. 80 (2019) 345–351.

[42] B. Jiang, W.J. Tao, H.Z. Dou, Y.L. Sun, H.M. Xiao, L.H. Zhang, N. Yang, A novel supported liquid membrane based on binary metal chloride deep eutectic solvents for ethylene/ethane separation, Ind. Eng. Chem. Res. 56 (51) (2017) 15153–15162.

[43] J. Kumełan, A.P.S. Kamps, D. Tuma, G. Maurer, Solubility of the single gases H₂ and CO in the ionic liquid [bmim][CH₃SO₄], Fluid Phase Equilibr. 260 (1) (2007) 3–8.

[44] Z.H. Tu, Y.Y. Zhang, Y.T. Wu, X.B. Hu, Self-enhancement of CO reversible absorption accompanied by phase transition in protic chlorocuprate ionic liquids for effective CO separation from N₂, Chem. Commun. 55 (23) (2019) 3390–3393.